A Micromachined Reconfigurable Metamaterial via Reconfiguration of Asymmetric Split-Ring Resonators

Yuan Hsing Fu, Ai Qun Liu, Wei Ming Zhu, Xu Ming Zhang, Din Ping Tsai, Jing Bo Zhang, Ting Mei, Ji Fang Tao, Hong Chen Guo, Xin Hai Zhang, Jing Hua Teng, Nikolay I. Zheludev, Guo Qiang Lo, and Dim Lee Kwong*

A micromachined reconfigurable metamaterial is presented, whose unit cell consists of a pair of asymmetric split-ring resonators (ASRRs); one is fixed to the substrate while the other is patterned on a movable frame. The reconfigurable metamaterial and the supporting structures (e.g., microactuators, anchors, supporting frames, etc.) are fabricated on a silicon-on-insulator wafer using deep reactive-ion etching (DRIE). By adjusting the distance between the two ASRRs, the strength of dipole–dipole coupling can be tuned continuously using the micromachined actuators and this enables tailoring of the electromagnetic response. The reconfiguration of unit cells endows the micromachined reconfigurable metamaterials with unique merits such as electromagnetic response under normal incidence and wide tuning of resonant frequency (measured as 31% and 22% for transverse electric polarization and transverse magnetic polarization, respectively). The reconfiguration could also allow switching between the polarization-dependent and polarization-independent states. With these features, the micromachined reconfigurable metamaterials may find potential applications in transformation optics devices, sensors, intelligent detectors, tunable frequency-selective surfaces, and spectral filters.

1. Introduction

Metamaterials are artificial composites which exhibit strong electric and magnetic responses to manipulate the amplitude, direction, polarization, wavelength, and phase of electromagnetic waves. By proper design of the unit cells, metamaterials have demonstrated amazing properties such as negative refraction,[1] super lens effect,[2] transformation optics,[3,4] chirality,[5] toroidal dipoles,[6] etc. Recently, reconfigurable metamaterials have attracted intense research interest since the active control of metamaterial characteristics is necessary to provide a flexible and versatile platform for mimicking fundamental physical effects.[7] In addition, the tunability could broaden the operation frequency range and enable reconfigurable metamaterial devices.[8,9] Tuning methods usually utilize capacitors/varactors,[10,11] semiconductors,[12] phase-change materials,[13,14] and ferromagnetic/ferroelectric materials.[15] However, most of these methods suffer from a limited tuning range as the variation of material properties is usually very small for the surrounding media and the metamaterial constituents. On the other hand, microelectromechanical systems (MEMS) technology has been well developed for fabrication and actuation of complicated micromechanical devices.[16,17] MEMS offers an ideal platform to directly reconfigure unit cells to overcome the limitations of the constituent materials.[18–20] As the unit cell is the fundamental building block of metamaterials, reconfiguration of the unit cell modifies the metamaterial properties and may promise unprecedented tunability. In our previous work,[20] a

Dr. Y. H. Fu, Prof. A. Q. Liu, Dr. W. M. Zhu, Prof. T. Mei, J. F. Tao
School of Electrical and Electronic Engineering
Nanyang Technological University
50 Nanyang Avenue, 639798, Singapore
E-mail: EAQLiu@ntu.edu.sg
Prof. X. M. Zhang
Department of Applied Physics
The Hong Kong Polytechnic University
Hung Hom, Kowloon, Hong Kong, P. R. China
Prof. D. P. Tsai
Department of Physics
National Taiwan University
1, Sec. 4, Roosevelt Road, Taipei 10617, Taiwan
Dr. H. C. Guo, Dr. X. H. Zhang, Dr. J. H. Teng
Institute of Materials Research and Engineering
3, Research Link, 117602, Singapore
Dr. Y. H. Fu, Dr. J. B. Zhang
Data Storage Institute
5, Engineering Drive 1, 117608, Singapore
Prof. N. I. Zheludev
Optoelectronics Research Centre
University of Southampton
Highfield, Southampton, SO17 1BJ, UK
Dr. G. Q. Lo, Dr. D. L. Kwong
Institute of Microelectronics
11 Science Park Road, 117685, Singapore

DOI: 10.1002/adfm.201101087

single split-ring resonator (SRR) was tuned by changing the gap between its two semisquare rings. Herein, two asymmetric split-ring resonators (ASRRs) are tuned by changing their separation distance, which dominates the coupling between both the electric and magnetic dipoles. The interactions between two adjacent ASRRs are demonstrated from the face-touch state to the back-touch state in real time. This reconfigurable metamaterial can be applied to many transmission-type applications which require normal incidence.

Two-dimensional (2D) metamaterials with one layer of metal pattern and another layer of dielectric substrate have been intensively studied experimentally thanks to their ease of fabrication.[21] However, a single layer of metal patterning makes it difficult to directly induce a magnetic response to normal incident light. An SRR with an asymmetric gap has been proposed as a paradigmatic design of a unit cell that would electrically induce the magnetic dipole.[22–24] The magnetic moment originates from the current loops in the fundamental inductive–capacitive (LC) resonant mode of the SRR. For this reason, the resonant frequency is strongly dependent on many factors that affect the current loops, such as the structure of a single SRR, the vertical coupling between stacked layers of SRRs,[25] and the lateral coupling of adjacent SRRs.[26–28] Among these factors, the lateral coupling of SRRs can be modified easily using micromachined actuators and also promises to be very efficient at tuning the metamaterial properties.

With this understanding, this paper demonstrates a reconfigurable metamaterial in which the unit cell is constructed using a pair of ASRRs. Previous work showed that induced magnetic-dipole resonance in the ASRR with two splits can only be excited by a normal incident wave when the polarization is perpendicular to the mirror line of the ASRR. This fact shows an important property of the "coherence" nature of the metamaterial, by adjusting the coupling between the ASRR.[24,29] Here, we investigate an ASRR with only one split and in which the symmetry is broken by displacing the gaps from the central line. Due to the asymmetry of the ASRR, a normal incident wave can excite a surface current loop to produce a magnetic dipole oscillation, regardless of the polarization direction of the normal incident wave. By adjusting the distance between two ASRRs using the micromachined actuators, the dipole–dipole couplings of both the magnetic field and the electric field are tuned simultaneously. These features provide the reconfigurable metamaterials with a unique merit of ability to wide tune the electromagnetic response.

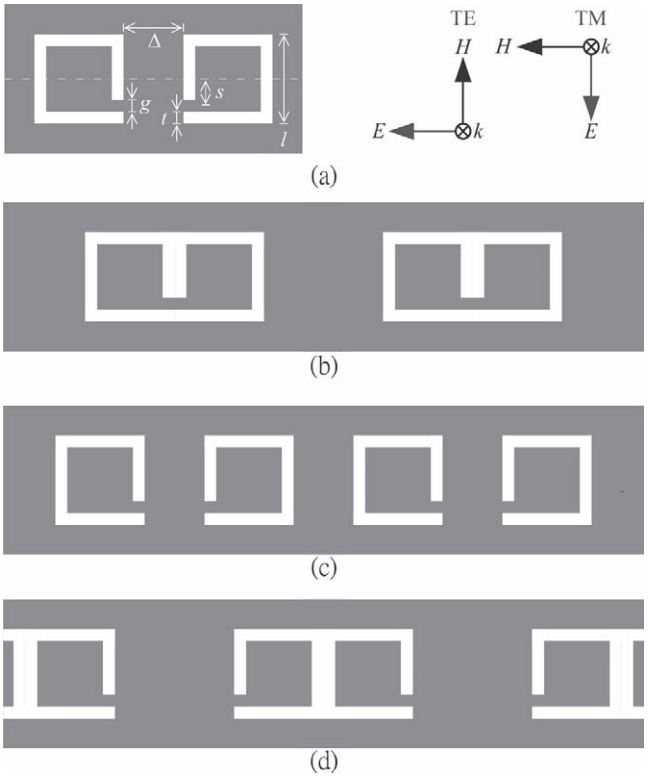

Figure 1. Schematic of the reconfigurable metamaterials. a) The gaps of the ASRRS are shifted from the central line by $s = 4.5$ μm. b–d) represent the unit cell in different configurations, b) for the face-touch state (i.e., $\Delta = 0$), c) for the separated state (i.e., $0 < \Delta < 20$ μm), and d) for the back-touch state (i.e., $\Delta = 20$ μm).

2. Results and Discussion

2.1. Design and Fabrication of the Unit Cell

The design of the unit cell for the reconfigurable metamaterial is shown in **Figure 1**a. The cell consists of a pair of square split rings with the split parts (i.e., the gaps) arranged opposite to each other. Asymmetry is achieved by displacing the gaps from the central line by $s = 4.5$ μm. As stated above, such asymmetry is essential to induce a magnetic dipole using the electric field component of normal incidence. The size of the unit cell is 50 μm × 25 μm ($L \times W$), and other dimensions are the sidewall length $l = 15$ μm, the width of the metal wire $t = 2$ μm, and the width of the gap $g = 2$ μm. The distance Δ between the paired ASRRs is an important tuning parameter since different configurations of the unit cell can be obtained by simply adjusting Δ. In an extreme case where $\Delta = 0$, the split rings touch face to face, which is called the face-touch configuration and is shown in Figure 1b. For $0 < \Delta < 20$ μm, the split rings are separated (called separated configuration) and their coupling strength varies with Δ. Figure 1c exemplifies a particular state of the separated configuration with $\Delta = 10$ μm. In another extreme case $\Delta = 20$ μm, the split rings touch back to back; this is called the back-touch configuration (Figure 1d). The diagrams in Figure 1b–d elucidate the key concept of micromachined reconfigurable metamaterials, namely, rearranging the metamaterial unit cell by simply displacing a part of the unit cell. For easy notation, the polarization of the incident wave is also indicated in Figure 1a. Transverse electric (TE) polarization state represents tthe case in which the electric field is perpendicular to the split side of the ring, while transverse magnetic (TM) occurs when the electric field is parallel to the split side.

The unit-cell design containing two oppositely arranged ASRRs has an intrinsic merit of high coupling between the two

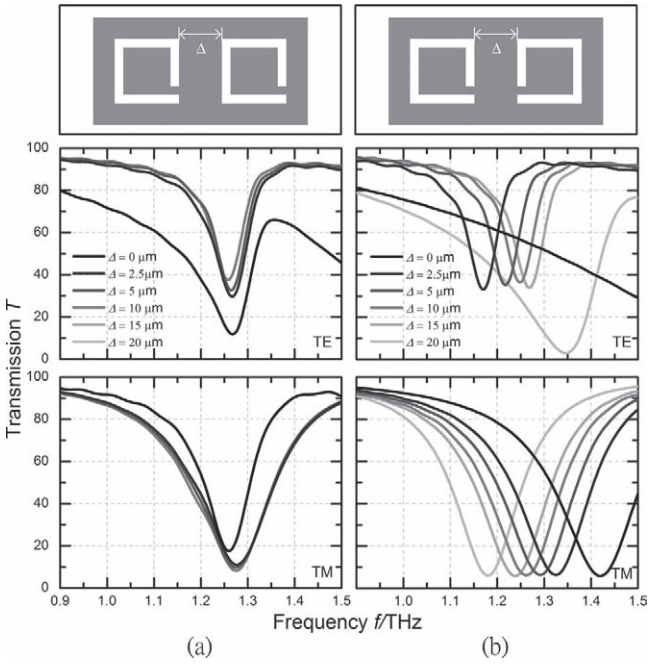

Figure 2. Transmission spectra of a) single ASRR and b) coupled ASRRs under TE- (upper row) and TM- (lower row) polarized incidence at various values of Δ. Δ was varied from 0 to 20 μm which is represented by the data curves from dark to light.

ASRRs and is thus expected to produce a wide tuning range, which is among the main interests of this work. For easy explanation of this feature, we compare this coupled ASRR design with another unit cell that is constructed by using two ASRRS with the same orientation, which equals to a single ASRR design (see **Figure 2**). In both designs, the coupling can be tuned by adjusting Δ. For the single ASRR design, resonant dips appear near 1.26 THz under the normal incidence of TE polarization (Figure 2a). However, the variation of Δ causes only a slight shift of the resonance frequency (0.6% at the maximum). Under the TM-polarized incidence, the shift of resonance dip is small also (0.8% at the maximum). Furthermore, changing Δ from 0 to 10 μm has the same effect as that of changing Δ from 20 to 10 μm due to the periodic symmetry of the unit cells, which further limits the tunability. In contrast, the coupled ASRR design exhibits very large tuning under either TE or TM incidence as shown in Figure 2b. For example, no LC-resonance dip occurs under TE polarization when Δ = 0 μm (see the upper panel of Figure 2b). We estimate that variation of Δ could cause > 20% shift of the resonance frequency, regardless of the polarization of incidence. This result verifies the large tunability of the coupled ASRRs and also shows the feasibility of reconfiguring the unit cells using the micromachined actuators.

The reconfigurable metamaterial and the supporting structures (e.g., microactuators, anchors, supporting frames, etc.) were fabricated on a silicon-on-insulator (SOI) wafer using deep reactive-ion etching (DRIE).[30] A close-up of the unit cell and an overview of the fabricated reconfigurable metamaterial are shown in **Figure 3**a and b, respectively. In the unit cell, one split ring is fixed while the other is movable. The fixed

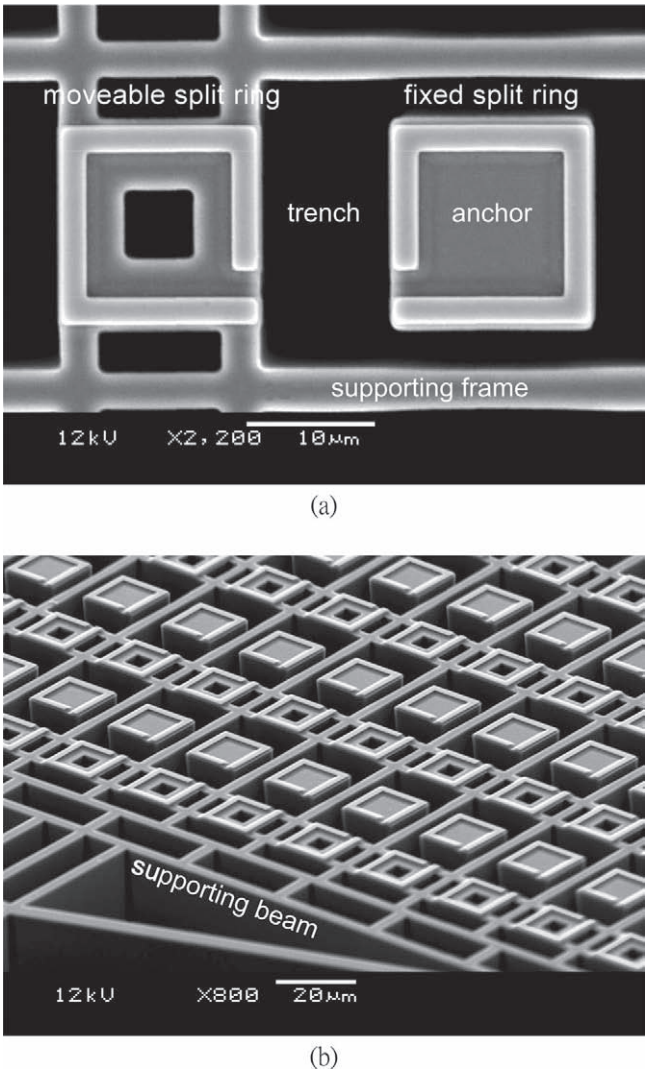

Figure 3. Scanning electron micrographs (SEMs) of the reconfigurable metamaterial. a) Close-up of the unit cell, which consists of a fixed split-ring resonator and a moveable ring. b) Overview of the reconfigurable metamaterial formed by an array of unit cells.

ring sits on an isolated anchor and the moveable one is on a floating frame connected to the comb-drive actuators with supporting beams. The split rings are formed by depositing and patterning an evaporated 500-nm aluminum layer. Some trenches surrounding the anchors are intentionally designed in to release the movable structures from the substrate and also provide space to move the supporting frame. The initial distance after fabrication is Δ = 10 μm. The reconfigurable metamaterial as shown in Figure 3b consists of 400 × 200 unit cells (footprint 1 × 1 cm); it employs two identical electrostatic comb-drive actuators on both sides for mechanically balanced translation of the supporting frame. Each comb-drive actuator provides a bidirectional in-plane translation following the actuation relationship $\Delta y = AV^2$, where Δy is the displacement, V the actuation voltage, and A = 0.05 μm V^{-2} is the actuation coefficient. The actuation range is from –10 to 10 μm, which corresponds to Δ = 0 to 20 μm.

2.2. Electromagnetic Response of the Reconfigurable Metamaterial

To characterize the electromagnetic response of the reconfigurable metamaterial, the transmission spectra of the metamaterials were measured using a terahertz time-domain spectrum (THz-TDS) system.[31] To understand the nature of the response, a simulation was also conducted using the finite diffraction-time domain (FDTD) solver. In the simulation, the electric conductivity of aluminum was chosen to be 2×10^7 S m^{-1} and the dielectric constant of the silicon substrate was 11.7. It is noted that although the surrounding media of the movable ASRR are different from those of the fixed ASRR due to the presence of the trenches and the supporting frame, the coupling effect is dominated by the relative positions between the ASRRs. In the numerical analysis, such substrate effect was taken into consideration.

The response to the TE normal incidence was first characterized. **Figure 4** shows both the measured and simulated transmission spectra in the frequency range of 0.9–1.5 THz for the TE polarization. The corresponding surface currents and magnetic-field components H_{normal} at resonance frequencies are also displayed on the right side of the spectra. Figure 4a represents the face-touch configuration and shows no LC resonance in the transmission spectrum. This absence can be explained by the observation that the surface currents on the two arms of the ASRR oscillate in parallel to the electric field and thus form no loop. Figure 4b shows the separated configuration in which Δ is tuned from 0 to 20 μm. In this configuration, circular surface current occurs on each ASRR, which results in two magnetic dipoles oscillating in phase. The quality factor (Q factor) of the resonance is approximately 13.8. When Δ = 2.5, 5, 10, and 15 μm, the resonant frequencies were positioned at 1.17, 1.21, 1.24, and 1.27 THz, respectively. An increase in Δ resulted in a blue shift of the resonant frequency. Figure 4c represents the back-touch configuration, and a broad resonance dip is present in the spectrum. It is observed that the surface currents on the contact sides (in the middle of the paired ASRRs) have near-zero amplitude, whereas those on the two arms oscillate in opposite directions and form a loop. The surface currents concentrate on the outside arms of the rings, which are similar to those of the asymmetric rings reported in previous work.[24]

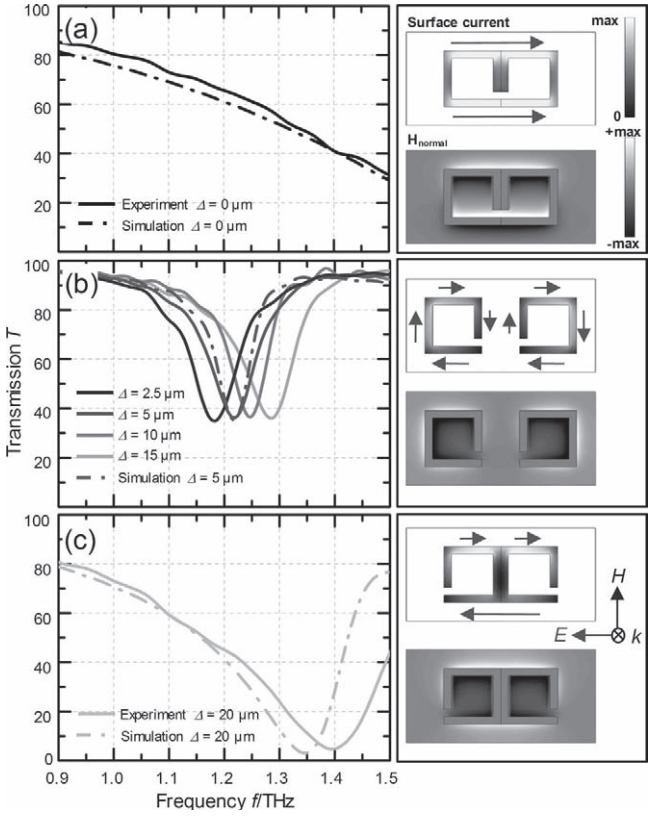

Figure 4. Transmission spectra for the TE polarization incident wave under the conditions of a) Δ = 0, b) Δ = 2.5, 5, 10, 15 μm (from dark to light) and c) Δ = 20 μm. The simulated surface currents and magnetic-field components H_{normal} are shown on the right side. The arrows and colors represent the directions and the intensities (the darker part shows the lower intensities and vice versa) of the surface currents (on the metal part), respectively. The maximum values of the surface current in (a), (b), and (c) were 0.015, 0.139, and 0.114 A m^{-1}, respectively. The maximum values of H_{normal} in (a), (b), and (c) were 0.012, 0.124, and 0.100 A m^{-1}, respectively. The values of the surface currents and H_{normal} were calculated assuming that the incident electric field was 1 V m^{-1}.

For TM polarization, the transmission spectra were also measured and simulated as shown in **Figure 5**. Because the electric field is oriented along a mirror plane for the ASRRs, the resonance is purely due to the electrical response, which is similar to the so-dubbed electric split-ring resonators (eSRRs).[32] In different unit-cell configurations, the circular surface currents are always excited but the two magnetic dipoles maintain a π phase shift, which results in a net zero magnetic dipole. However the frequency tuning is associated with the interaction of the two antiparallel magnetic dipoles. The resonant dips for Δ = 0, 2.5, 5, 10, 15, and 20 μm appear at 1.42, 1.32, 1.29, 1.24, 1.22, and 1.16 THz, respectively. The resonant frequency tends to have a red shift, which is opposite to the blue shift for the TE polarization, with increasing values of Δ. The Q factor of TM polarization (electric dipole resonance) for the separated configuration is approximately 7.8, which is approximately half of the Q factor of the TE polarization (LC resonance) under the same conditions.

2.3. Real-Time Tuning of Electromagnetic Response

To demonstrate the real-time tuning capability of the micromachined reconfigurable metamaterial, the tuning of the resonance dip under dynamic actuation was also characterized. The tuning time from minimum to maximum distance was experimentally determined to be about 500 μs, which corresponds to an operational frequency of 1 kHz. The Doppler effect is trivial in this case since the speed (0.04 m s^{-1}) was ten orders of magnitude smaller than the speed of light. Therefore, the responses in the real-time tuning process can be represented by the spectra of different static states. The simulated contour maps of the transmission at different time intervals are shown in **Figure 6** for both TE and TM polarization. It can be seen clearly that with the increase of time (and consequent larger values of Δ), the belt of resonance dips curves upwards for the TE polarization but bends down for TM polarization. Moreover, the belt of resonance dips for the TE polarization is

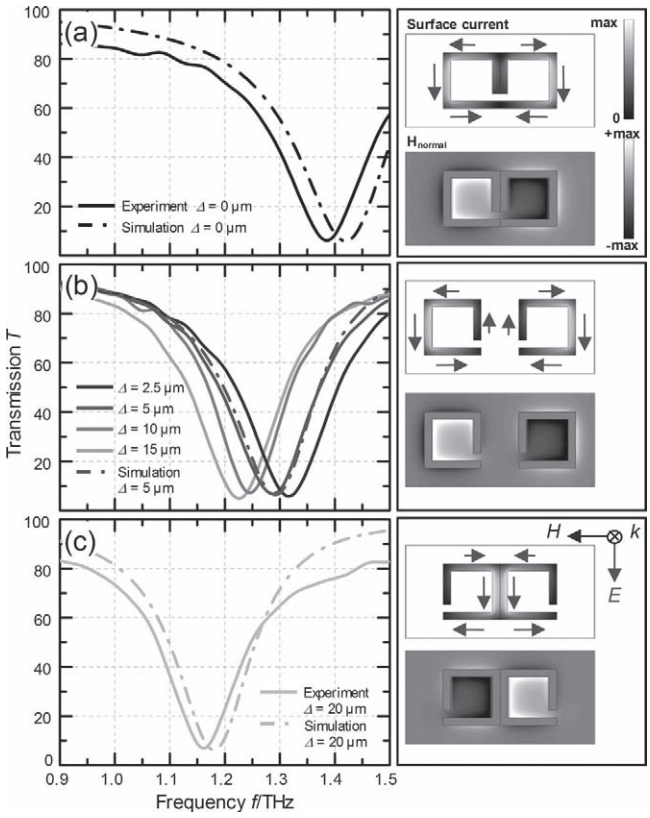

Figure 5. Transmission spectra for the TM polarization incident wave at a) $\Delta = 0$, b) $\Delta = 2.5$, 5, 10, 15 μm (from dark to light), and c) $\Delta = 20$ μm. The simulated surface currents and magnetic field components H_{normal} are shown on the right side. The arrows and the colors represent the directions and the intensities (the darker part shows the lower intensities and vice versa) of the surface currents (on the metal). The maximum values of the surface currents in (a), (b), and (c) are 0.103, 0.096, and 0.105 A m^{-1}, respectively. The maximum values of H_{normal} in (a), (b), and (c) are 0.092, 0.085, and 0.094 A m^{-1}, respectively. The values of the surface currents and H_{normal} were calculated assuming that the incident electric field was 1 V m^{-1}.

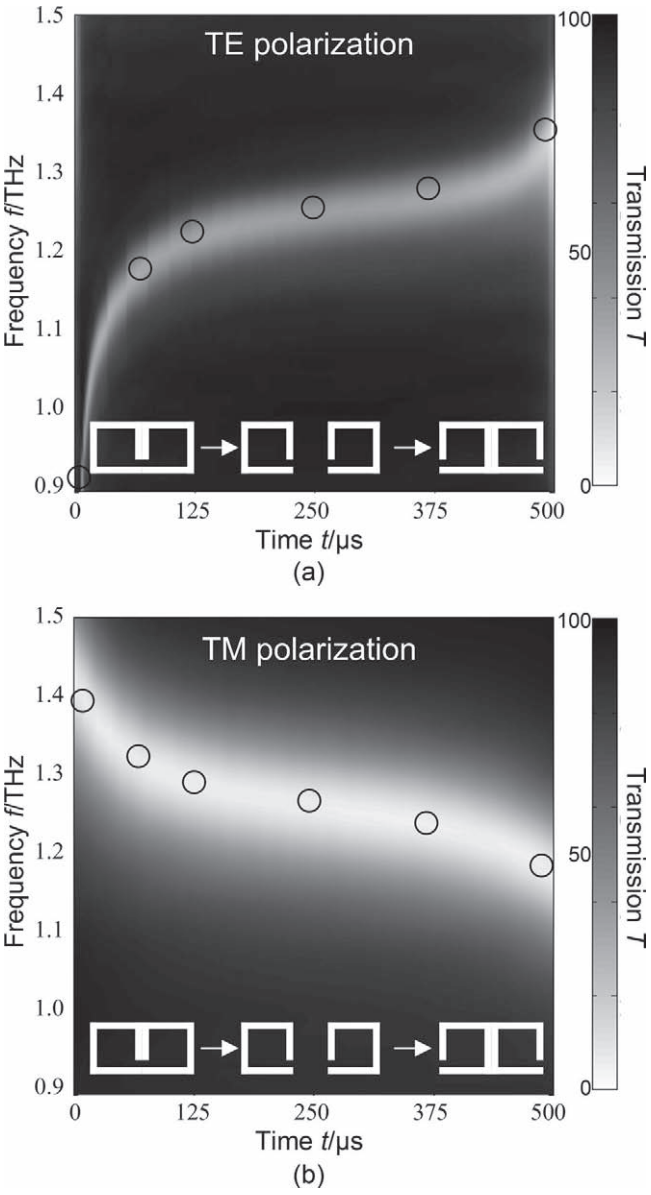

Figure 6. Real-time tuning of the transmission spectra as represented by the contour maps of transmission as functions of time and frequency for a) TE polarization and b) TM polarization. The circles represent the measured data points of resonance frequencies shown in Figure 4 and Figure 5. The insets indicate the changes of unit-cell configurations.

narrower (which corresponds to a higher Q factor) than that for the TM polarization. This distinction can be attributed to the differences in the excited electric and magnetic dipoles and the dipole–dipole coupling. More specifically, for the TE polarization the two electric dipoles are excited antiparallel at the gap whereas the two magnetic dipoles are in-phase in the center of the ASRR (see Figure 4b); for the TM polarization the opposite is true (see Figure 5b). The electric dipole coupling dominates the frequency shift when the tuning time is less than 250 μs, and the magnetic dipole coupling dominates thereafter. For transverse dipole–dipole coupling, the interaction of the parallelly oriented electric dipoles (in TM polarization) decreases the resonance frequency with increasing Δ.[27] The electric dipole–dipole coupling dominates this interaction, which results in the downwards trend of the belt of resonance over a tuning time from 0 to 250 μs, as shown in Figure 6b. For a tuning time between 250 to 500 μs, the two antiparallelly oriented magnetic dipoles become closer (in TM polarization), which tends to further decrease the resonance frequency. When the tuning time is approximately 250 μs, both the electric and magnetic dipole coupling are relatively weak, which results in a slight tuning of resonance frequency. Unlike with TM polarization, the electric dipoles are antiparallelly oriented while the magnetic dipoles are parallelly oriented, which results in a blue shift of the resonance frequency. For TE polarization, the tuning range of the resonance frequency is from 0.98 to 1.28 THz, which corresponds to a change of approximately 31% of the initial resonance frequency. For TM polarization, the tuning range of the resonance frequency is from 1.15 to 1.40 THz (approximately 22%). For easy comparison, the measured resonant dips (see Figure 4 and Figure 5) are superimposed onto

the contour maps. A reasonable agreement of the resonance positions is achieved between the simulation and the measurement. It is interesting to see that, at a particular time interval of 250 μs (corresponding to $\Delta = 10$ μm), the resonant dips of the TE and TM polarization overlap. This overlap is of profound importance since the response is polarization independent; it demonstrates the unique potential of the reconfigurable metamaterials in switching from a polarization-dependent state to a polarization-independent state for electromagnetic response, although the Q factors are not the same due to the asymmetry of the gaps in the split rings.

3. Conclusions

A reconfigurable metamaterial is presented by reconfiguring the unit cell, which consists of a pair of asymmetric split-ring resonators. The coupling distance between the pair of ASRRs is tuned by bidirectional micromachined actuators. Due to the asymmetry of the ASRRs, the inductive-capacitive resonance can be excited by a normal incident terahertz wave. The reconfigurable metamaterial not only has a wide tuning range of the resonance frequency up to 31% and 22% for the TE and the TM polarization, respectively, but also produces a high quality-factor resonance and an in-phase magnetic-dipole oscillation for the TE polarization. In the process of dynamic tuning, the reconfigurable metamaterial can be switched from the polarization-dependent state to the polarization-independent state. The metamaterial may find potential applications in transformation optics devices, sensors, intelligent detectors, tunable frequency-selective surfaces, and spectral filters.

4. Experimental Section

The transmission spectra characterization of the reconfigurable metamaterials was performed using a terahertz time-domain spectrum (THz-TDS) system. 100-fs optical pulses centered at 800 nm at a repetition rate of 76 MHz from a mode-locked Ti:sapphire laser were focused onto a photoconductive antenna of low-temperature-grown GaAs to generate the terahertz wave. A Fourier transform was used to extract the frequency spectrum from the time-domain data. A time range of the time-domain data was chosen to exclude Fabry-Pérot fringes that arise from the substrate. The transmission spectra were normalized with respect to the transmission of the pure silicon substrate (i.e., T_{sample}/T_{Si}).

Acknowledgements

This work was supported by the Science & Engineering Research Council (SERC) of A*STAR Singapore with project Metamaterials Programme: Nanoplasmonics (Grant No. SERC 092 154 0098) and EPSRC (UK).

Received: May 16, 2011
Revised: June 21, 2011
Published online:

[1] D. R. Smith, D. C. Vier, N. Kroll, S. Schultz, *Appl. Phys. Lett.* **2000**, *77*, 2246.
[2] N. Fang, X. Zhang, *Appl. Phys. Lett.* **2003**, *82*, 161.
[3] U. Leonhardt, *Science* **2006**, *312*, 1777.
[4] J. B. Pendry, D. Schurig, D. R. Smith, *Science* **2006**, *312*, 1780.
[5] A. V. Rogacheva, V. A. Fedotov, A. S. Schwanecke, N. I. Zheludev, *Phys. Rev. Lett.* **2006**, *97*, 177401.
[6] T. Kaelberer, V. A. Fedotov, N. Papasimakis, D. P. Tsai, N. I. Zheludev, *Science* **2010**, *330*, 1510.
[7] N. I. Zheludev, *Science* **2010**, *328*, 582.
[8] H. T. Chen, W. J. Padilla, J. M. O. Zide, A. C. Gossard, A. J. Taylor, R. D. Averitt, *Nature* **2006**, *444*, 597.
[9] H. T. Chen, J. F. O'Hara, A. K. Azad, A. J. Taylor, R. D. Averitt, D. B. Shrekenhamer, W. J. Padilla, *Nat. Photonics* **2008**, *2*, 295.
[10] K. Aydin, E. Ozbay, *J. Appl. Phys.* **2007**, *101*, 024911.
[11] I. Gil, J. Garcia-Garcia, J. Bonache, F. Martin, M. Sorolla, R. Marques, *Electron. Lett.* **2004**, *40*, 1347.
[12] K. A. Boulais, D. W. Rule, S. Simmons, F. Santiago, V. Gehman, K. Long, A. Rayms-Keller, *Appl. Phys. Lett.* **2008**, *93*, 043518.
[13] M. J. Dicken, K. Aydin, I. M. Pryce, L. A. Sweatlock, E. M. Boyd, S. Walavalkar, J. Ma, H. A. Atwater, *Opt. Express* **2009**, *17*, 18330.
[14] Z. L. Samson, K. F. MacDonald, F. De Angelis, B. Gholipour, K. Knight, C. C. Huang, E. Di Fabrizio, D. W. Hewak, N. I. Zheludev, *Appl. Phys. Lett.* **2010**, *96*, 143105.
[15] L. Kang, Q. Zhao, H. J. Zhao, J. Zhou, *Opt. Express* **2008**, *16*, 8825.
[16] H. Cai, A. Q. Liu, X. M. Zhang, J. Tamil, D. Y. Tang, Q. X. Zhang, C. Lu, *Appl. Phys. Lett.* **2008**, *92*, 031105.
[17] W. M. Zhu, X. M. Zhang, A. Q. Liu, H. Cai, T. Jonathan, T. Bourouina, *Appl. Phys. Lett.* **2008**, *92*, 251101.
[18] H. Tao, A. C. Strikwerda, K. Fan, W. J. Padilla, X. Zhang, R. D. Averitt, *Phys. Rev. Lett.* **2009**, *103*, 147401.
[19] W. M. Zhu, H. Cai, T. Mei, T. Bourouina, J. F. Tao, G. Q. Lo, D. L. Kwong, A. Q. Liu, *IEEE Int. Conf. on Micro Electro Mech. Syst., Tech. Dig., 23rd (Hong Kong)* **2010**, 196.
[20] W. M. Zhu, A. Q. Liu, X. M. Zhang, D. P. Tsai, T. Bourouina, J. H. Teng, X. H. Zhang, H. C. Guo, H. Tanoto, T. Mei, G. Q. Lo, D. L. Kwong, *Adv. Mater.* **2011**, *23*, 1792.
[21] W. Withayachumnankul, D. Abbott, *IEEE Photonics J.* **2009**, *1*, 99.
[22] J. B. Pendry, A. J. Holden, D. J. Robbins, W. J. Stewart, *IEEE Trans. Microwave Theory Tech.* **1999**, *47*, 2075.
[23] R. Singh, I. A. I. Al-Naib, M. Koch, W. L. Zhang, *Opt. Express* **2010**, *18*, 13044.
[24] V. A. Fedotov, M. Rose, S. L. Prosvirnin, N. Papasimakis, N. I. Zheludev, *Phys. Rev. Lett.* **2007**, *99*, 147041.
[25] N. Liu, H. Liu, S. N. Zhu, H. Giessen, *Nat. Photonics* **2009**, *3*, 157.
[26] M. Decker, S. Linden, M. Wegener, *Opt. Lett.* **2009**, *34*, 1579.
[27] N. Feth, M. Konig, M. Husnik, K. Stannigel, J. Niegemann, K. Busch, M. Wegener, S. Linden, *Opt. Express* **2010**, *18*, 6545.
[28] I. Sersic, M. Frimmer, E. Verhagen, A. F. Koenderink, *Phys. Rev. Lett.* **2009**, *103*, 213902.
[29] N. Papasimakis, V. A. Fedotov, Y. H. Fu, D. P. Tsai, N. I. Zheludev, *Phys. Rev. B* **2009**, *80*, 041102.
[30] J. Li, A. Q. Liu, Q. X. Zhang, *Sens. Actuators A* **2006**, *125*, 494.
[31] H. C. Guo, X. H. Zhang, W. Liu, A. M. Yong, S. H. Tang, *J. Appl. Phys.* **2009**, *106*, 063104.
[32] D. Schurig, J. J. Mock, D. R. Smith, *Appl. Phys. Lett.* **2006**, *88*, 041109.